High Intensity Femtosecond XUV Pulse Interactions with Atomic Clusters: Final Report

Principal Investigator
Todd Ditmire
Department of Physics
The University of Texas at Austin
2515 Speedway Stop C1510
Austin, TX 78712
Phone: 512-472-3296
E-mail: tditmire@physics.utexas.edu

Administrative Point of Contact: LaKesha Henry
Phone: 512-471-1485
E-mail: lakesha.henry@utexas.edu

DOE/Office of Science Program Office: Basic Energy Sciences (BES), AMO Physics;
Chemical Sciences Program
DOE/Office of Science Program Office Technical Contact: Thomas Settersten
Phone 301-903-8428
E-mail: Thomas.Settersten@science.doe.gov

DOE Award Number: DE-FG02-03ER15406
DOE Report/Product Number: DOE-UTCHEDS-15406
Research area: (k) Atomic, Molecular, and Optical Sciences
October 12, 2016

1. Introduction

Atomic clusters have long been studied by chemists and physicists because of the unique position that clusters hold as an intermediate state between molecules and solids [i]. Many studies have traced the properties of materials from their monatomic characteristics to their solid state characteristics through an examination of the material as it forms larger and larger clusters. Many of these studies have been undertaken on van der Waals bonded clusters. Such atomic clusters can be formed from the atoms or molecules in a gas when the gas expands from high pressure in a gas jet into vacuum [ii]. The cooling associated with the gas's adiabatic expansion can be sufficient to cause nucleation of the gas particles into clusters. Small clusters can also be formed from the laser driven ablation of solids [iii,iv] or small particles [v,vi,vii].

Quite recently, the nature of cluster interactions with intense, short wavelength light, ie vacuum ultraviolet and extreme ultraviolet, have come under study. Such studies are now possible because of the development of a number of intense, ultrafast sources in the XUV and X-ray range. For example, free electron lasers operating in the 100 - 10 nm wavelength range are now available [viii] and the recent activation of the LCLS makes experiments at photon energies of greater than 1 keV possible [ix]. These FELs yield pulses with energy of 0.1 - 1 mJ and focused intensity of 10^{14} - 10^{16} W/cm^2. The advances in high order harmonic generation with femtosecond terawatt lasers also opened the possibility of XUV experiments at high intensities. Such studies are the subject of the work performed in this grant and described here.

One of the fundamental science questions that has arisen about the irradiation of clusters by intense XUV or X-ray radiation is how the atoms within the cluster are ionized and what ionic charge state is produced. Another question includes whether the cluster then explodes by a simple Coulomb explosion, like that expected when many electrons are removed from the cluster on a femtosecond time scale, or whether the cluster expands more slowly like the hydrodynamic expansion of a hot gas. In the context of wanting to understand how proteins might explode, additional questions can be asked about how clusters of mixed atomic species clusters explode and how the light ions (like H) interact with the heavier, more slowly expanding ions (such as C and O).

To address some of these fundamental questions, under this program we constructed at UT a new XUV beam line and target chamber in which high-order harmonics of our upgraded 40 TW 30 fs Ti:sapphire laser (the THOR laser) were increased in energy by more than a factor of 25. The intensity at 38 nm, the primary wavelength of the studies decribed in this final report, approached 10^{14} Wcm^{-2}. Using this beam line we first verified the previous results on Xe and Ar clusters and then expanded measurements of CH_4 and Xe doped CH_4 clusters to compare with clusters measured at LCLS by our group. We present in the progress section preliminary analysis of this data. Our results with this high-harmonics beam line using a 38 nm pulse continue to show anomalously high charge states in the time-of-flight (TOF) spectra of Xe and Ar [x]. We also observed what appeared to be a hydrodynamic explosion in Xe clusters while Ar and methane appeared to tend more toward a Coulomb explosion [xi]. We have also completed the construction of a new target source employing the Laser Ablation of Microparticles (LAM) in an

aerosol to produce metal and metal oxide and metal oxide clusters (nanoparticles) with a very narrow size distribution.

2. Background and Motivation for the Studies Performed

2.1 Clusters in Intense XUV and X-ray Pulses

At the core of this proposal is a study of intense femtosecond short wavelength pulse interactions with clusters and the explosions that they drive. These studies are motivated by a number of factors. In a fundamental sense, these experiments rest in a dramatically different physical regime than previous investigations of high intensity near-IR interactions with clusters. This can first be characterized by considering the Keldysh parameter, $\gamma = (U_p/2I_p)^{1/2}$. As is well known in strong field physics, ionization dynamics in an atomic system are dominated by tunneling when γ <1 and dominated by multi-photon processes when γ >1. A similar statement can be made with regards to collisional heating in a plasma if I_p is replaced by the photon energy $h\nu$; in the former case heating occurs by quasi-classical electron-ion scattering and in the latter the heating is described by individual photon absorption. Most studies of laser-cluster interactions over the past ten years have been made with large ponderomotive energy (γ is small). This is illustrated in Fig. 2.1 where the band of photon energy and laser intensity is outlined. Most of the large literature on high intensity light interactions with clusters rests in the yellow band on this plot. Our goal in the program we first proposed in the previous funding period of this grant was to push these studies off the yellow band. Ultimately we would like to explore the regime where the intensity is high (> 10^{13} W/cm^2) but where γ is now greater than 1. In this regime, electron dynamics are *not* dominated by ponderomotive energies.

Early molecular dynamics simulations by Hadju *et al.* suggested that the LCLS pulse may be too long to beat the expansion of a large biological molecule which is similar to a cluster [xii]. They

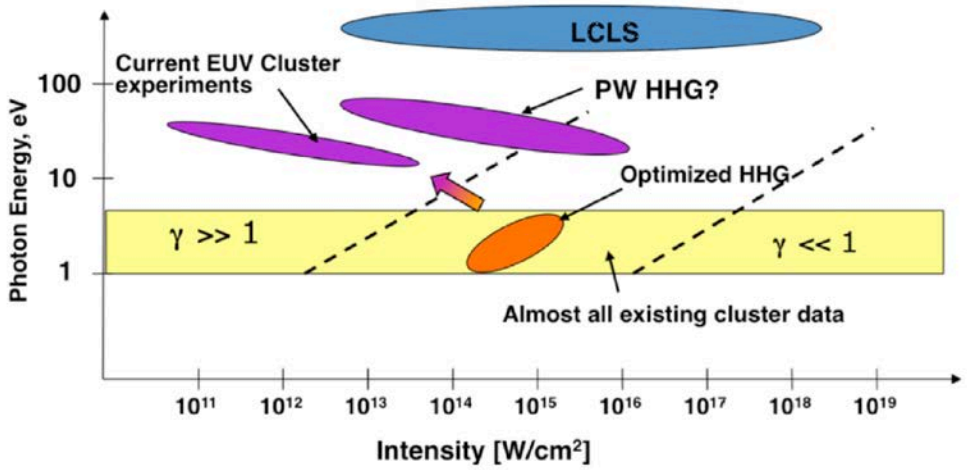

Figure 2.1: Plot of intensity and photon energy for cluster irradiation experiments. The yellow band illustrates the photon energy region of previous studies and the purple oval illustrates the region for our proposed experiments.

based these conclusions on particle dynamic simulations which treated all ionization as vertical, where every electron leaves the cluster once an atom or ion in the cluster is freed by photo- or Auger ionization. The resulting ionized cluster explodes by Coulomb forces. However, a more detailed study and subsequent simulations of this physics indicates that this picture is too pessimistic. In our recent cluster experiments at LCLS, we found that photo-ionized electrons freed by the multi-keV photons of the LCLS pulse will leave such a molecule/cluster immediately until sufficient charge is accumulate so as to retain photo electrons and the lower energy Auger electrons. In fact, space charge forces will confine most of these electrons and the low ponderomotive energy of the short wavelength LCLS field will be insufficient to eject these electrons from the cluster. So the cluster may explode not by the Coulomb explosion mechanism but instead may explode by electron driven hydrodynamic expansion, a mechanism in which the explosion time scale may be dramatically longer than in the Coulomb explosion regime, particularly if the electron temperature in the cluster remains low (below, say, 100 eV). In our methane cluster experiments we observed a transition between a Coulomb explosion for small clusters to hydrodynamic explosion for larger clusters.

With this background and discussion in mind, it is instructive to consider the characteristics of exploding clusters subject to intense femtosecond irradiation by IR, XUV and X-ray pulses. A table summarizing the comparison of these characteristics is presented in Table 1. The first major difference between IR irradiation of clusters and XUV or X-ray irradiation rests with the initial ionization mechanism for the constituent atoms. When the Keldysh parameter is less than 1, as it is in the IR experiments, initial ionization is dominated by tunneling ionization, with the above threshold ionization heating which accompanies this process. In the short wavelength field, initial ionization will be by photo-ionization, with additional energy given to the electrons based on photon energy and ionization potential. XUV irradiation will photo-ionize the cluster atoms by removing electrons from the outermost shell while X-ray irradiation will produce electrons via inner shell ionization. In either case, the average energy of the ejected electrons is given by the photon energy and initial ionization potential. How the constituent atoms in a cluster are ionized in the intense XUV pulses is the first major question that the work proposed here will address.

The next major question involves whether a cluster nano-plasma is formed in the interaction. Do electrons liberated by ionization from the cluster's atoms become ejected from the cluster immediately or are enough held in by space-charge forces that the clusters evolution is affected by this electron cloud, or "fluid" if a purely plasma physics formalism is applied? The question is complex and depends very much on the size and atomic constituents of the cluster. It is now well established in clusters larger than a few hundred atoms that such nano-plasmas tend to form when an IR pulse irradiates these clusters at intensities up to 10^{18} W/cm^2 (though low Z-clusters, such as hydrogen clusters tend not to form nano-plasmas [xiii]). How this electron plasma formation affects the explosion of the clusters is well explored in the IR regime. If a nano-plasma does form, the cluster tends to expand hydrodynamically (discussed in the next section). Whether such a nano-plasma will be formed in the x-ray (LCLS) regime is an open question as electrons produced by photo-ionization may have energies of a large fraction of 1 keV and can likely be ejected from the cluster. We therefore expect a partial Coulomb explosion. Given our preliminary experiments on Xe and Ar clusters in the XUV regime discussed in this report, we believe that a nano-plasma is formed, at least in intermediate to large (>100 atom) Xe and Ar clusters at modest XUV intensity.

IR laser irradiation $h\nu$~1.5 eV	XUV laser irradiation $h\nu$~10-100 eV	X-ray laser irradiation $h\nu$>1keV at LCLS
Tunnel ionization	Sequential photo-ionization	Inner shell photo-ionization followed by Auger emission
U_p > surface potential substantial e- stripping Coulomb expansion	U_p << surface potential e- confined Hydrodynamic expansion	U_p << surface potential substantial e- stripping Mostly Coulomb expansion
Giant dipole resonance at low e- density n_{crit} ~ 10^{21} cm^{-3}	Giant dipole resonance at solid density n_{crit} ~ 10^{23} cm^{-3}	Resonance occurs above solid density n_{crit} ~ 10^{25} cm^{-3}
Hot electron (>1 keV) production possible through stochastic heating	Very little hot electron production	Hot electron (>1 keV) production possible through photo-electron ejection
Nano-plasma collisionless T_e ~U_p~10-100 keV	Very collisional T_e~1-30 eV >>U_p	Collisionality not known

Table 1: Comparison of characteristics if cluster irradiation in an XUV and an IR field

The IR field often exhibits a ponderomotive energy well above the binding potential of the cluster (above 1 keV for intensities greater than 10^{16} W/cm^2), leading to a rapid stripping of many of the ionized electrons in the cluster. This leads to disassembly of the cluster by a Coulomb explosion. In contrast, the XUV pulses will exhibit very low ponderomotive energy, with U_p below 1 eV for even rather intense (>10^{14} W/cm^2) pulses with a wavelength shorter than 100 nm. We expect a greater preponderance of electrons to be trapped in the cluster which will tend to expand by electron thermal hydrodynamic forces. Consequently, the electron temperature in the cluster plays a much greater role in the driving the speed of the expansion. However, as the photon energy further increases from the XUV to the X-ray regime we expect that photo-ionization will produce electrons with sufficient energy for ejection from the cluster (followed by lower energy Auger electrons which may or may not be trapped in the cluster). We might expect a transition from ponderomotive dominated heating of cluster nano-plasmas in the IR regime, to the production of cold, electron confined cluster nano-plasmas in the XUV regime, returning, ultimately to highly charged clusters with significant electron ejection in the x-ray regime.

The XUV created nano-plasma is quite different than the nano-plasma created in an IR irradiated cluster. Because of the low ponderomotive energy and modest photon energy we expected a much lower electron temperature when XUV pulses were used. In addition, further tunnel ionization can occur to higher charge states in the IR field, however, photo ionization will be stopped in the XUV pulse as the ions are stripped to charge states with ionization potentials which exceed the photon energy (with the additional complication of local ion field enhancement of the ionization). As we have discovered in the work presented here, the cluster nanoplasma produced after ionization appears to affect the atomic structure significantly, resulting in a

correction to the ionization potential that opens single photon ionization to charge states higher than would be possible for single atoms.

Another interesting difference rests in the density at which the drive field will come into resonance with any collective giant dipole oscillations of the electrons confined to the cluster. This dipole resonance can be thought of as a collective oscillation of the confined electron cloud about the positively charged ion sphere formed from the ions in the irradiated cluster [xiv]. It has a frequency of $\omega_p/3^{1/2}$ where ω_p is the standard plasma frequency. In IR laser pulses, the frequency of the giant resonance matches the laser frequency at a density of about 5×10^{21} cm^{-3}. This density is well below the density of the solid density cluster once the constituent atoms become even only singly ionized. Therefore, a femtosecond laser pulse interacts with this nano-plasma well away from the giant resonance during most of the interaction. It has been well established that when intense IR pulses are employed to irradiate a cluster, the cluster plasma density is well above the critical density for the laser, and the cluster must expand to lower the density to around 5×10^{21} cm^{-3} to bring it into resonance. By this time, the cluster is large and the low density plasma is not very collisional, a situation which supports a collective oscillation, an effect which has well defined signatures in the high field IR/cluster interaction. In contrast, an XUV pulse, with wavelength of ~ 30 nm will be in resonance at solid density, $>5 \times 10^{23}$ cm^{-3}. This density will appear before the cluster has expanded but after the constituent atoms have been completely ionized by the pulse. So we expect that collective oscillation effects potentially to play a role in XUV/cluster interactions, as they do in IR pulses. However, the much greater collisionality of the nano-plasma at the density of the collective resonance in the XUV and the low electron temperature of the photo-ionized plasma lead to a quite different response than that seen in IR experiments, where the resonance occurs in a cluster plasma of density two orders of magnitude lower.

2.3 Atomic Physics Effects in Dense Cluster Nano-Plasmas

One of the salient aspects of high intensity pulse interactions with clusters, whether the pulses are at IR wavelengths, XUV of X-ray wavelengths, is that the atomic structure of the atoms in the cluster is affected by the local environment in the cluster. A significant experimental consequence of this perturbation of the atomic structure is in the charge state distribution that results from the irradiation of the clusters. The local fields in the cluster affect the ionization rates of the atoms and ions, and collisions further affect the ionization state through collisional ionization and the opposite process of recombination.

It has been well known for many years that the charge states observed from the intense irradiation of clusters by IR and near UV pulses lead to the production of charge states in the clusters which are far higher than the charge states observed during the interaction of the same intensity pulses with single atoms [xv,xvi]. The origins of this effect were debated for some time but the consensus at this point is that while some enhancement of the tunnel ionization rate of single atoms in the laser field occurs because of the local fields an atom sees in the cluster from nearby ions, the predominant reason for high charge state production is because of collisional ionization of the cluster ions by heated electrons in a cluster nano-plasma. It is generally accepted that using simple collisional ionization rates combined with a model for the effective electron temperature

of the cluster electrons can explain the high charge states seen in high intensity IR cluster experiments.

A different picture emerges when ionization of the atoms in a cluster by short wavelength pulses is considered. The first observation of "anomalously" high charge states in clusters irradiated at high intensity by an XUV pulse occurred in the first experiments performed at DESY on the FLASH FEL. In this experiment Xe clusters of sizes ranging up to ~30,000 atoms/cluster were studied [5-8] and subsequent experiments on Ar clusters have been published as well. In the first experiments, performed at wavelength near 95 nm at intensities of ~10^{13} W/cm^2, a surprising result was found in which high ion charge states were observed, with ions of charge up to 8+ being measured [xvii]. Later experiments at 95 nm showed electron emission from moderate sized (~1000 atom) Ar and Xe clusters with a quasi-Maxwellian distribution with a 9 eV electron temperature [xviii]. More recent experiments at 33 nm in small (<100 atom) clusters have also been reported, with a different conclusion [xix]. In those experiments at shorter wavelength the electron removal from the cluster was purely sequential, and that authors saw little evidence for the production of a nano-plasma or a thermal electron distribution.

These FLASH experiments generated a number of theoretical studies, focused in particular on the reasons for the high charge state production and anomalously high absorption seen in the DESY experiments. There were at least three distinct models advanced to explain the DESY results. Santra and Greene proposed that the large absorption of VUV irradiated clusters and high charge states observed can be explained by a thermalized nano-plasma heated by inverse bremsstrahlung absorption with appropriately corrected collision rates [xx]. Siedschlag and Rost posited that the high charge states are produced by single photon absorption in the cluster facilitated by the distortion of the ionic binding potential by the neighboring ions and passing electrons in the cluster [xxi]. In its simplest form this picture can be described by Fig. 2.2 (reproduced from their paper) in which single photons can ionize atoms formed from an array of nearby ions. The numerical model from this group was later improved to include the effects of space-charge confined electrons in the cluster as well as the fields from the neighboring ions [xxii]. Finally, Jungreuthmayer et al. performed simulations which indicated that the high charge states result from collisional ionization by an electron cloud heated through a process they refer to as many-body recombination heating [xxiii]. In the models of Santra et al and Jungreuthmayer *et al.* no account of the distortion of an atomic potential is taken, and the FLASH are explained simply on the basis of collisional ionization by a heated cluster nano-plasma. As Fig. 2.2 illustrates, this is likely to be a significant omission.

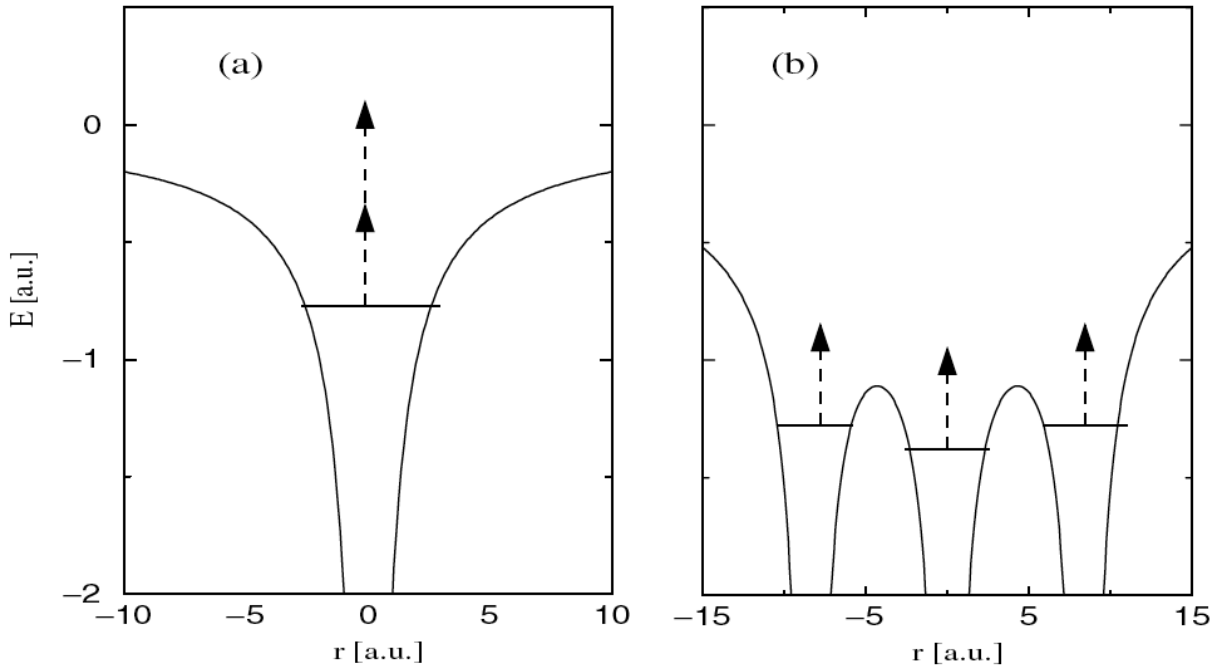

Figure 2.2: Illustration of how ions in a cluster can be ionized by a single XUV photon when their effective ionization potential is lowered by the presence of nearby ions.

Based on experiments we have performed on Xe clusters with our harmonics XUV source described in this report, we have forwarded a slightly different explanation for the formation of high charge states in these clusters. Our picture is in essence similar to the physical picture of Rost et al. in which we believe that the high charge states are predominantly produced by single photon ionization of atoms whose ionization potential is strongly depressed in the fields of the nearby electrons and ions in the cluster. By lowering the ionization potential through local field interactions, it is possible for the high flux of XUV photons to ionize to high charge states by sequential multiple ionization, with charge states with field-free ionization potential normally above the incident photon energy now becoming ionized through this potential lowering.

The numerical model that Rost et al. has published captures much of this physics. However, it is possible to gain quantitative insight by applying a statistical mechanical approach to the ionization potential lowering. If one can assume that a dense cluster nano-plasma is formed, which seems to be the case based on our explosion ion spectra, the well established plasma physics description of ionization potential lowering can be applied. A quantitative description is based on the picture illustrated in Fig. 2.3. When an electron is liberated from an atom or ion in a plasma, it is not removed to infinity but is placed into the environment of the surrounding plasma. Because of the attractive potential of the sea of ions and the repulsive potential of the plasma electron "fluid" the potential energy of the liberated electron will be different than an electron removed to infinity (where its potential is zero). Calculating this potential energy of an electron inserted into a plasma yields the amount by which the ionization potential is effectively lowered.

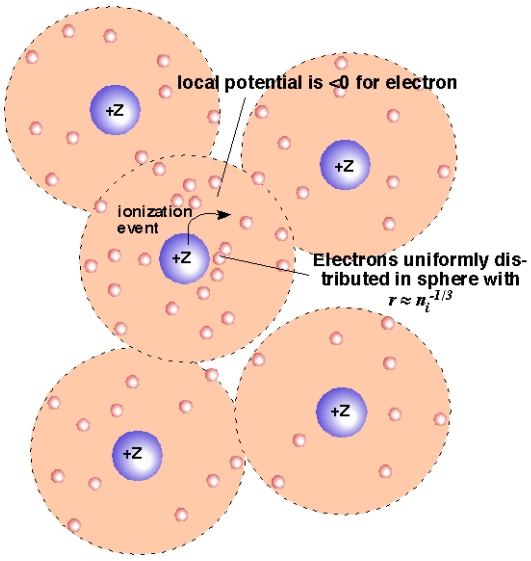

Figure 2.3: A plasma physics picture of ionization potential lowering views the ionization of an ion in a plasma as the removal of an electron from a bound state in the ion and insertion of that electron into the local electron fluid. The lowering of the ionization potential is then the difference between the potential of an electron at infinity and its potential in the plasma fluid (which is negative).

The most commonly applied model is that in which the plasma electrons are assumed to form a Debye sheath around the ions and the liberated electron is injected into the exponential radial electron density around an ion. In this situation, it can be shown that the effective continuum level for the electrons is lowered by [xxiv]

$$\Delta I_p^{(Debye)} = 2Z^{3/2}e^3\sqrt{\frac{\pi n_i}{k_B T_e}} \qquad (1)$$

where n_i is the ion density, T_e is the plasma electron temperature and Z is the effective average charge state of ions in the plasma. This model is based on the view of electron "shielding" around each ion with an effective radial electron distribution that has an exponential profile with a 1/e fall-off range given by the Debye length. The weakness of this model is that it relies on a plasma in which there are many electrons in the Debye sphere, a situation met in plasmas that are hot and not of particularly high density. An XUV irradiated cluster is expected to produce a nano-plasma with rather high density, in excess of solid density with multiple ionization and modest temperature. We therefore expect that this traditional plasma continuum lowering formula to be inaccurate in our experiments. In these kinds of plasmas, often referred to as strongly coupled plasmas, the usual way to treat the situation is like that depicted in Fig. 2.3: assume that all previously ionized electrons are uniformly distributed around each ion. In that case, the electrostatic continuum lowering is independent of temperature (because the Coulomb potential energy of the plasma exceeds its thermal energy) and can be written as [xxv]:

$$\Delta I_p^{(SC)} = \frac{9}{10}(2Z-1)e^2 n_i^{1/3} \qquad (2)$$

This formula indicates that the extent of continuum lowering is nearly proportional to the average ionization state in the plasma and might be expected to be significant in clusters, such as Xe, where high ionization is expected. For example, a Xe cluster ionized to Z~4+ will exhibit continuum lowering of 24 eV according to eq. 2.

This is sufficient to allow higher charge state production simply by single photon ionization at the photon energies we employ in the experiments proposed here. The confirmation that continuum lowering affects photo ionization of atoms in clusters is one of the central goals of the experiments proposed here and described below.

2.4 Cluster Explosion Mechanisms

The next major physics we studied in our work surrounded the mechanism for the explosion of the clusters under intense irradiation. The mechanisms for cluster explosions in intense IR fields are well established. When the clusters are small and composed of low Z ions, electrons are not confined to the cluster and are stripped by the ponderomotive forces of the laser. In this case, a Coulomb explosion occurs. The ejected ions have an energy which is determined principally by the potential energy that the ions have in their equilibrium position in the cluster (provided that the laser rise time is fast enough to strip the clusters faster than the ions can expand [xxvi]). At the other extreme, when large, high-Z clusters are irradiated the confinement of a large fraction of electrons by space charge forces results in the creation of the previously discussed nano-plasma. The explosion is driven mainly by electron fluid pressure resulting in an ion energy spectrum that be explained by the fluid equations describing a two-fluid (electron and ion) plasma. When a sizeable fraction of the electrons leave, what likely occurs is the formation of a quasi-neutral core in the cluster surrounded by a charged shell [xxvii]. Consequently the ion energy distribution is formed from a Coulomb explosion component and a slower, hydrodynamic component. Which of these pictures is relevant to the XUV and X-ray experiments is an open question.

The limits of behavior exhibit distinct ion energy spectra. The expansion of a spherical plasma hydrodynamically will yield an ion energy spectrum with that is roughly given as [xxviii]

$$f(E)dE = E^{-1/2}e^{-6E/kT_e} \qquad (3)$$

The shape of the ion spectrum is linked to the temperature of the electrons in the nano-plasma (if they can indeed be described as a Maxwellian.) In this view, the initial size of the cluster is not important. On the other hand, if electrons are extracted, or have enough energy to leave the cluster sphere by overcoming any space charge attraction, a spherical cluster of ions stripped to charge Z will have an ion energy distribution upon explosion of

$$\begin{aligned} f(E)dE &= E^{1/2}dE \quad & E \le E_{MAX} \\ &= 0 & E > E_{MAX} \end{aligned}$$

where $E_{MAX} = Z^2 n_i e^2 r^2 / 3\varepsilon_0$ is the maximum ion energy which occurs for ions on the surface of the sphere of radius r. Because the ion energy spectrum in this case does depend on cluster size, typically observed ion spectra from clusters exploding through this Coulomb explosion mechanism, result from a convolution of this single cluster ion spectra with a cluster size

distribution [xxix]. It is an excellent approximation for most van der Waals bonded clusters to assume that the cluster size distribution is a Log-normal distribution with a width very nearly equal to the mean cluster size. Because of the difference in the ion spectra from these two mechanisms, its possible to differentiate them through the measurement of the shape of the spectra of the exploding clusters. Fig. 2.4 illustrates data from our work on exploding Xe clusters irradiated by high intensity 38 nm wavelength pulses. An attempt to fit these data with a curve based on the Coulomb explosion model only succeeds for the lowest ion energies, while the majority of the energy range, from 100 to 500 eV, is instead fit by a curve from a hydrodynamic expansion of an 8 eV plasma. From this we can conclude that the majority of clusters (at least the larger ones in the distribution) seem to explode by hydrodynamic forces of a cool 8 eV plasma, though there is a number of small (~100 atom) clusters which explode by Coulomb explosion.

How clusters explode in intense short wavelength fields is critical in determining the time scale of the cluster explosion. As illustrated in Fig. 2.4, we have seen evidence for a hydrodynamically driven explosion in large Xe clusters irradiated by intense 38 nm pulses while, as discussed below, Ar clusters under similar conditions seem to exhibit a Coulomb component. Further exploring this physics in the XUV, not only in homo-nuclear clusters like Ar and Xe but also in mixed species clusters, like CH_4 is a central part of this proposal. In fact, we expect that in some circumstances, including mixed species clusters like methane, that there will be an outer shell of ions which are ejected by Coulomb explosion, led by the light H^+ ions in the case of methane clusters [xxx,xxxi], while the inner core expands as a quasi-neutral nano-plasma.

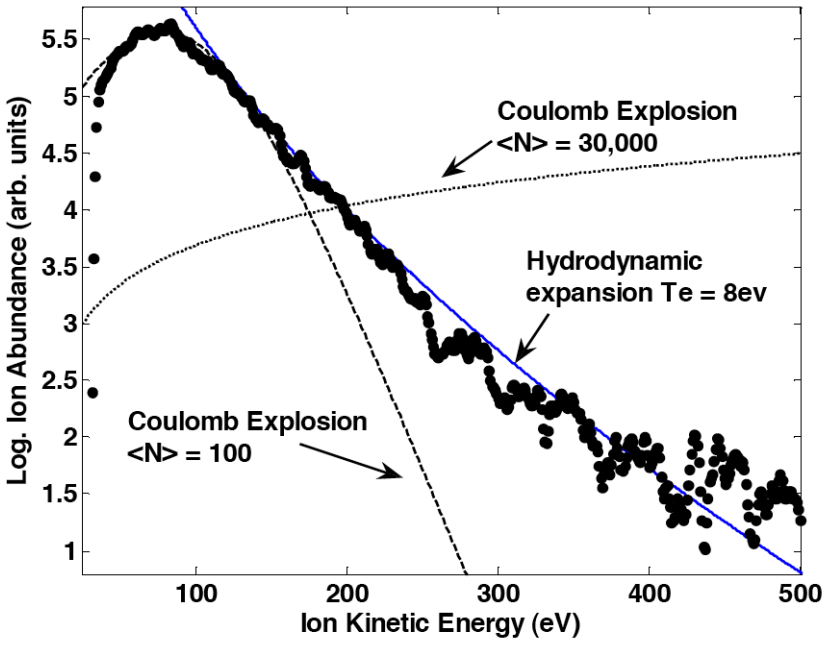

Figure 2.4. Ion energies measured by drift TOF. The cluster size expected for the temperature and pressure of the expansion is <n> = 30,000. A Coulomb model fits the data only when assuming <n> = 100.

3.0 Work Performed Under this Grant

3.1 Explosion of Clusters Heated by the free-electron laser LCLS

We measured explosions of Ar, Xe, CH_4, CD_4 and mixed CH_4/Xe clusters (mean sizes up to 10^5 molecules) using the free-electron, x-ray laser at LCLS at intensities approaching 10^{17} Wcm^{-2}. Understanding these interactions was relevant to experiments imaging biological molecules, protein nanocrystals, DNA or viruses. For all of the clusters we studied, the interaction with the intense keV photons were dominated initially by single photon photo-ionization and by Auger emission following each inner shell photoionization event. The exit of electrons from the cluster successively builds a positive charge until the space charge potential confines the photo- and Auger electrons. A charged layer of ions forms at the surface of the cluster while a quasi neutral, plasma core fills in the center whose temperature is determined by the photo- and Auger electron energies distributed over all the plasma electrons[xxxii].

The formation of the nanoplasma leads to rapid three-body recombination during hydrodynamic explosion of the inner core. We find that the maximum charge states produced in the Xe clusters, Xe^{26+} at the highest intensities, was virtually identical to the highest charge states observed from single Xe atoms irradiated under identical conditions. On the other hand, photoionization of Xe clusters produced a large number of Xe^{+} and Xe^{2+}, charge states virtually absent in the ion charge state spectra of single Xe atoms irradiated under identical x-ray pulse conditions. Furthermore, we found that the mean kinetic energy per ion-charge state for charge states < Xe^{8+} remained almost constant when increasing the intensity from $4.5x10^{14}$ W/cm^2 to $6x10^{16}$ W/cm^2. Finally, we observed that the distribution function of ion kinetic energies also remained the same for the wide range of intensities employed and has the functional dependence on energy of a plasma which has expanded hydrodynamically. A simple rate equation model, which included the effects of photoionization heating, hydrodynamic expansion, and ion-electron recombination qualitatively explained the production of lower charge states in the Xe clusters and the observed electron temperatures. We have completed a draft of a long paper on this research which includes additional data on Xe clusters for laser pulse widths of 3 fs, 60 fs and 150 fs over the same range of intensities.

We have also completed analysis of the CH_4 and CD_4 data and completed a letter paper on CH_4 [xxxiii]. Similar to Xe clusters, the x-ray interaction with methane clusters is dominated by photoionization of the inner ($1s^2$) shell of carbon (the photoionization cross section of H is three orders of magnitude smaller than C for 850 keV photons) but the subsequent filling of the hole and Auger emission of valence-bond electrons results in the dissociation of hydrogen as protons, rather than an increased charge state of the carbon.

When the cluster size is increased, ion states formed within the cluster produced broadened peaks because ions emitted in the forward and backward directions in the TOF have different arrival times dependent upon the distribution in ion energy. Though ion with charge states to C^{6+} are observed in molecular targets in our experiment, these peaks do not broaden in the TOF with increased cluster size, hence they are not produced significantly in clusters. To produce high charge states of carbon all of the protons must be removed from the molecule first, and this delay suppresses their formation in the cluster.

We find strong peaks from CH_5^+, $C_2H_4^+$, and $C_2H_9^+$ due to association of recoil protons and hydrocarbon ions with neutral molecules at the solid densities of the clusters. Similar to results for Xe clusters, methane clusters form a positive outer shell with increasing total charge until the

space charge potential is sufficient to retain the photo- and Auger electrons. Within the positive shell a neutral plasma is formed, and we find dissociative recombination plays an important role in the population of CH_5^+ and larger molecules. The resulting Coulomb explosion of the outer shell becomes dominated by protons because their expansion is more rapid than hydrocarbon ions because of their smaller mass[xxxiv]. The plasma core expands much more slowly increasing the importance of electron-ion recombination (which is rapid at solid densities, see Ref. xxxii).

For 3 fs laser pulses of 2 keV photons, we observed that the smallest ion energies were observed for the cluster sizes of 10^3 and 10^4 molecules. For these pulses we expect less than 4% of the molecules to be ionized. While the formation of CH_5^+ and larger molecules might disturb the possibility for x-ray diffraction imaging of the cluster, or comparably a biological molecule, molecular fragmentation occurs only after Auger emission (hole lifetime ~7.5 fs) and well after the end of the laser pulse. If effect the hollow molecule formed by the laser delays atomic motion that would distort imaging.

3.2 High Energy XUV pulse production by HHG on the Texas Petawatt Laser

We completed preliminary measurements of XUV pulse energies when 100J pulses of the Texas Petawatt laser (150 J, 150 fs at wavelength of 1057 nm) were focused into a large aperture gas jet. We performed one 4-week run on the Texas Petawatt. The set-up for the experiment is illustrated

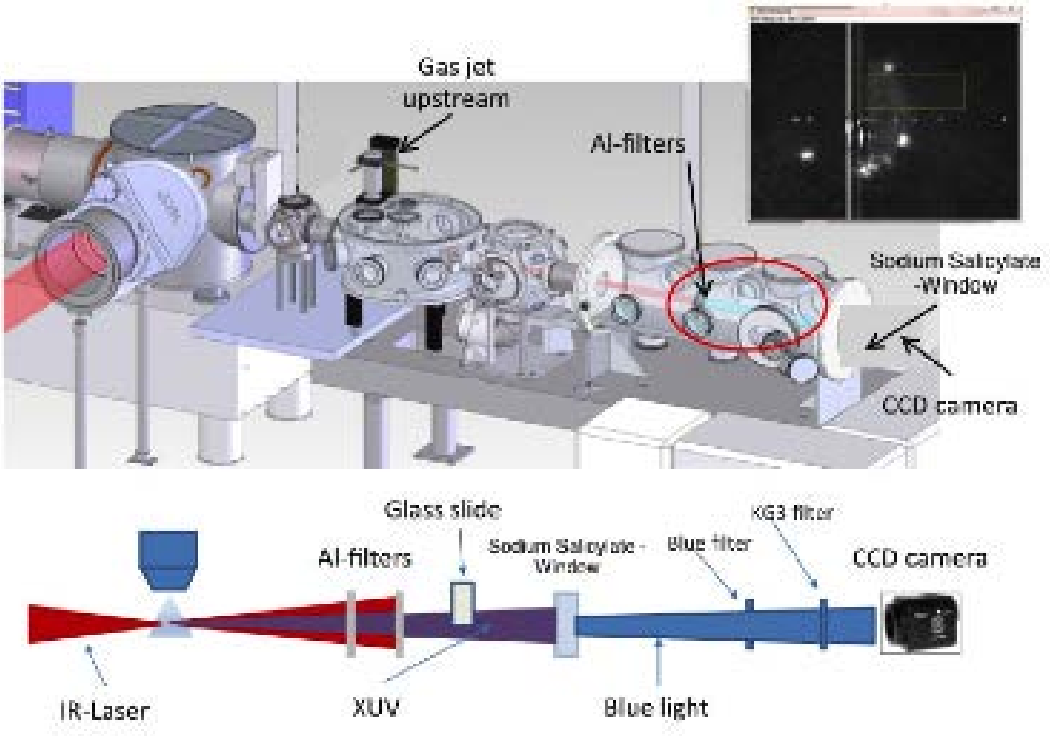

Figure 3.1: Layout of the HHG conversion experiment on the Texas Petawatt Laser. Inset: image of XUV light partially obscured on the Salicylate detector.

in figure 3.1. We focused the laser with an f/40 mirror into a specially built slit gas jet which produced nearly a cm^2 of gas for a target. The laser light was filtered away with expendable Al filters. The XUV light was incident on a XUV sensitive window which had a calibrated yield. A window could be inserted to ascertain if through light from the laser was responsible for the observed signal. The inset to figure 3 shows an HHG beam partially obscured by the window proving that the signal was not IR or optical light. Estimates on the per harmonic yield indicate that we produced 30 – 100 μJ of energy per harmonic in the transmission window of the Al filter.

A major difficulty in this experiment was the separation of the harmonics from the petawatt of IR light using only sacrificial filters. To reduce the IR fluence the 2 cm diameter filters were placed 2 m from the harmonic gas jet. The limited solid angle of collection made detection of the XUV light uncertain at the once per hour laser shot rate. We are planning a second experiment that will block the center of the laser beam and focus the resulting donut beam into the harmonic jet. This approach is used successfully on the harmonic beamline used with the THOR laser.

3.3 Upgrade of THOR, New Beamline for Harmonic Generation, and Target Chamber

We completed an upgrade of the THOR laser at UT and the construction and testing of a new beam line for high-harmonic generation (HHG). The upgrade of THOR included replacing the regenerative amplifier with optical parametric amplification (OPA) using BBO crystals. This amplifier has greatly increased the contrast of the laser, increase the output to 1.2 J, and shortened the pulse to 30 fs at a 10 Hz repetition frequency.

In our past experiments on XUV irradiation of noble gas clusters we produced harmonic radiation by loosely focusing 40 fs pulses with a MgF f#/60 lens from our THOR Ti:sapphire laser into an Ar gas jet. We were able to produce an 8μm spot dia. with the 38 nm pulse, yielding a focal intensity of ~ 10^{11} W/cm^2 assuming an XUV pulse duration of 10 fs. These harmonics were then focused into the plume of a second, low density cluster jet. The main limitation of this apparatus was that the drive laser pulse energy was limited to ~ 60 mJ by the use of lens and focal geometry constrained by the lab space. This limited the XUV energy per pulse at the target to ~ 0.1 nJ/pulse in the 21^{st} harmonic.

We have now improved this beam line in new expanded lab space. This new beam line is illustrated in Figure 3.2. It is an all reflective design where the THOR laser sends its full energy (~1.2 J) loosely-focused (*f*#140) into a gas jet to produce HHG of significant intensity. The XUV is sent to the interaction chamber where one of the harmonics is selected and focused using a Sc/Si mirror into gas clusters or nanoparticles for HED studies.

F

Figure 3.2: THOR XUV beamline spanning across two laboratory spaces.

Figure 3.3 shows a top view of the XUV beamline and the compressor chamber. The beamline is divided in three stages: 1- Focusing, 2- HHG, 3-XUV interaction. In the first stage the compressed 3.8 cm diameter beam is steered 90º in the focusing chamber, sent to a 0º mirror in the retro chamber. There, the beam reflects back onto a *fl* = 5.50 m, concave spherical mirror that focuses the beam under a rectangular shaped (~0.5 mm x 5 mm) conical, gas jet in the HHG stage at fundamental intensities up to $3x10^{15}$ W/cm^2. The jet is moved upstream of the focus to keep the intensity near this transition for relativistic motion of quiver electrons. The angle of incidence in the focusing mirror is about 1º which makes spherical aberrations at focus negligible ($1/e^2$ spot diameter of 76 μm, 5.5 mm Rayleigh length). Two stages of differential pumping are used upstream of the harmonic nozzle to limit the pressure to below 10^{-5} Torr in the compressor. Three stages of differential pumping are used downstream to limit the pressures to less than 10^{-7} Torr. At a distance one focal length from the gas jet the fundamental and low harmonics are blocked and high harmonics sent to the XUV interaction chamber. A selected Sc/Si mirror picks a particular harmonic in the 10-60 nm range and focuses it on a gas jet.

Separation of the XUV pulses from the fundamental and low harmonics is done in a two-step process. Initially, the pulse before leaving the compressor goes through a 1 cm diameter mirror (reflective mask) in the center of the beam that creates a donut shape spatial beam profile. This disk is at approximately two focal lengths upstream from the focusing mirror and its image is located at two focal lengths. At this location, right before entering the interaction chamber, an aperture with the size of the circular disk blocks most of the infrared donut shape profile. The XUV, having a much smaller wavelength and divergence propagates through the center of the aperture with a small fraction of the fundamental light that was scattered by the gas jet. Following the aperture, a 200 nm aluminum foil (Luxel Corp.), with approximately 20-50% transmission in the XUV range blocks the remaining fundamental light and low harmonics. Optimization of the HHG yield is achieved by observing the harmonic spectrum using a grazing incident spectrograph with a multichannel plate detector, phosphor plate, and CCD camera. We first varied the location of the gas jet with respect to the laser focus at the maximum fundamental energy. A series of vacuum tubes with different length are swapped before or after the HHG chamber to produce the coarse positioning (2" steps) along the laser beam while a xyz-manipulator for the gas jet and translator for the focusing mirror provides fine adjustment. We optimized the HHG production as a function of jet pressure, x-y position of the jet relative to the focus, pulse width of the laser (optimum at minimum pulse width), and laser energy (optimum at maximum fundamental energy). Using an XUV calibrated photodiode (AXUV576C, Opto Diode Corp.) we measured the total energy on target in the 21st harmonic (38 nm) to be up to 5 nJ (average over 100 shots) with shots up to 20 nJ. This is a factor of 25 times greater than measured for the previous beam line (Ref. 5 below). We performed a knife edge measurement of the XUV focus for the Si/Sc mirror which is consistent with a spot diameter of 4 μm at $1/e^2$ and a peak laser fluence of 80 mJcm^{-2} Given adjacent, coherent 19th and 23rd harmonics we expect the overall XUV envelope in time (Δt~7 fs) to be modulated, leading to peak intensities on the order of 10^{14} Wcm^{-2}.[xxxv]

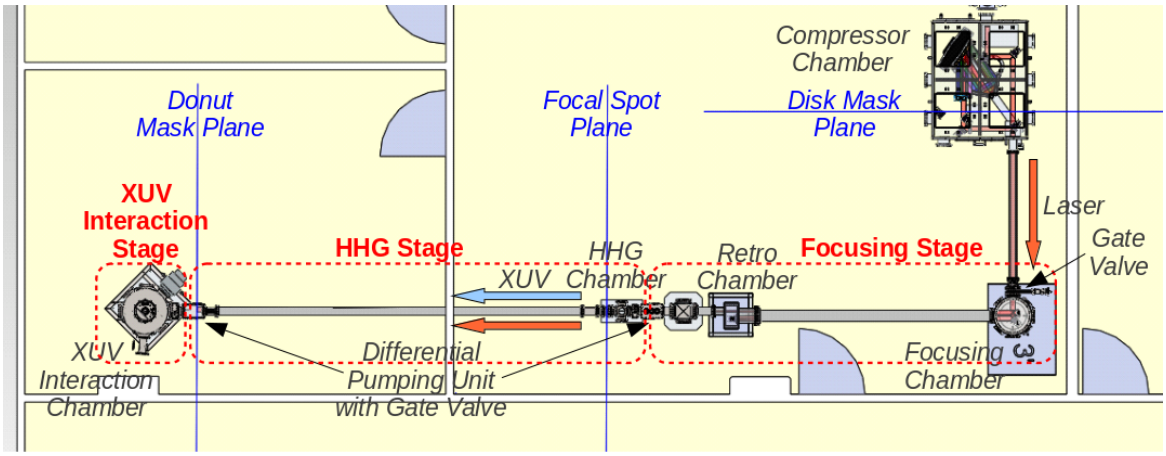

Fig. 3.3. Top view schematic of the new XUV beamline.

3.4 Gas Cluster Explosion Dynamics Using XUV Light Generated on THOR

Our previous experiments on the interaction of intense near-infrared laser pulses with noble gas clusters have shown the ejection of anomalously high ion charge states, and revealed that the clusters' explosion mechanism (either Coulombic or hydrodynamic) depends on the cluster size and Z constitution [xxxvi, xxxvii]. While the interaction of these clusters with infrared has been extensively explored, the effects of shorter wavelengths like extreme ultraviolet (XUV) have not. In this regime individual photons carry enough energy to eject bound atomic electrons via photoionization. In the previous contract period we complete experiments to look at Ar and Xe clusters at XUV wavelengths and Ar, Xe, CH_4, CD_4 and Xe doped CH4 using x-rays at the free-electron laser LCLS.

We have used the newly constructed THOR-XUV beamline to study the explosion dynamics of Ar and Xe clusters to compare with our previous XUV experiments and for CH_4 and Xe doped CH_4 to compare with our data from the LCLS experiments. We have also completed preliminary experiments on Van der Waals clusters of O_2 and CO_2 to compare with the planned experiments measuring the ionization potentials of oxygen ions in crystalline oxide nanoparticles.

This XUV pulse is then separated from the infrared beam and focused in the XUV Interaction Stage, shown in Figure 3.4. In this chamber, as seen in Figure 1B, a Sc/Cr/Si multilayer mirror with 12.5 cm focal length into another gas jet that produces gas clusters. This focusing mirror also selects the 21st harmonic (38 nm, 32.6 eV) among the broad distribution of harmonic frequencies produced in the HHG process. The energy of the focused XUV was measured using an XUV photodiode and the spot size measured by a knife edge experiment, and it was found that the energy is about 5 nJ and the focus size is about 5μm at $1/e^2$.

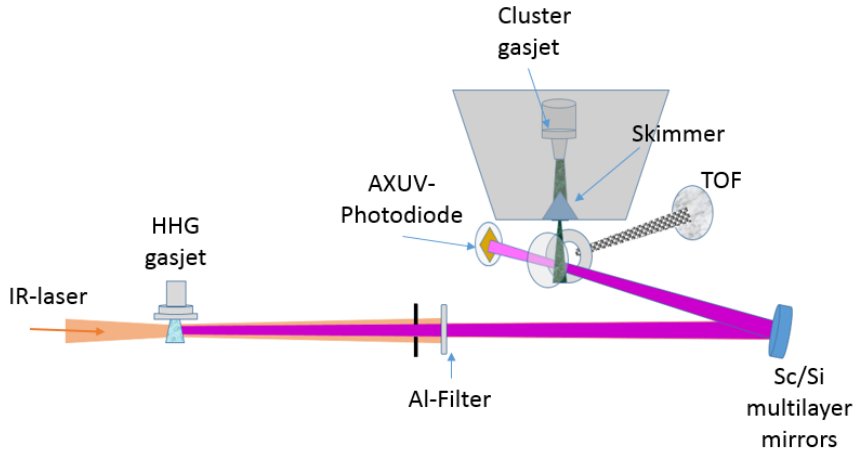

Figure 3.4: Top view of the schematic of the interaction setup.

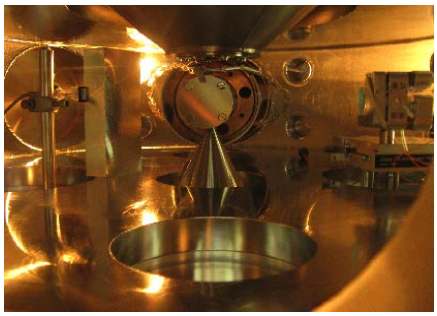

Figure 3.5: Photograph inside of the chamber with the end of the accelerating grids of the TOF at the center. The jet propagates between the grids to a skimmer observed below. The Si/Sn mirror is seen on the right. The XUV beam propagates across the chamber from the left, outside of the grids to hit the focusing Si/Sn mirror observed on the right. The mirror focuses the XUV light to the center of the grids.

The produced cluster size can be controlled by changing the nozzle backing pressure and temperature, and the use of a cryo-jacket to cool the nozzle to temperatures as low as 100K to reach the larger cluster sizes. A skimmer is used to send a narrow stream of clusters into the interaction region, where the exploded cluster fragments are observed using a Wiley-McLaren time-of-flight (TOF) spectrometer (Figure 3.5). This new TOF is completely shielded by mu metal to eliminate the effects of magnetic fields. Because of a longer drift region, it also has proven better resolution. For the ion TOF we applied voltages to the TOF grids to accelerate the ions, while for the ion and electron kinetic energies, we grounded the grids allowing the ions or the electrons to fly free through the drift region, and then the particles are detected using an MCP with its output read by a fast oscilloscope.

We conducted multiple experiments on the XUV chamber with Ar, Xe, CH_4, Xe doped CH_4, N_2, O_2, CO_2 and SF_6 clusters, measuring the ion time of flight, the ion kinetic energy and the electron kinetic energies produced by the exploding clusters. Our initial run was performed using Argon gas, for which the average cluster size was varied between 10 atoms to 7 million atoms.

We used the Hagena parameter to estimate the average cluster size. We used the Ar cluster experiment to calibrate and optimize the TOF by changing the voltage on the front grids as well as the voltage on the MCPs. Figure 3.6 shows (TOF) data from XUV irradiation of the peak associated with Ar^+, where it is clear from the peak-widths that the explosion energy increases as a function of the average cluster size (the asymmetry is due to a misalignment of the laser focus with respect to the axis of the TOF spectrometer).

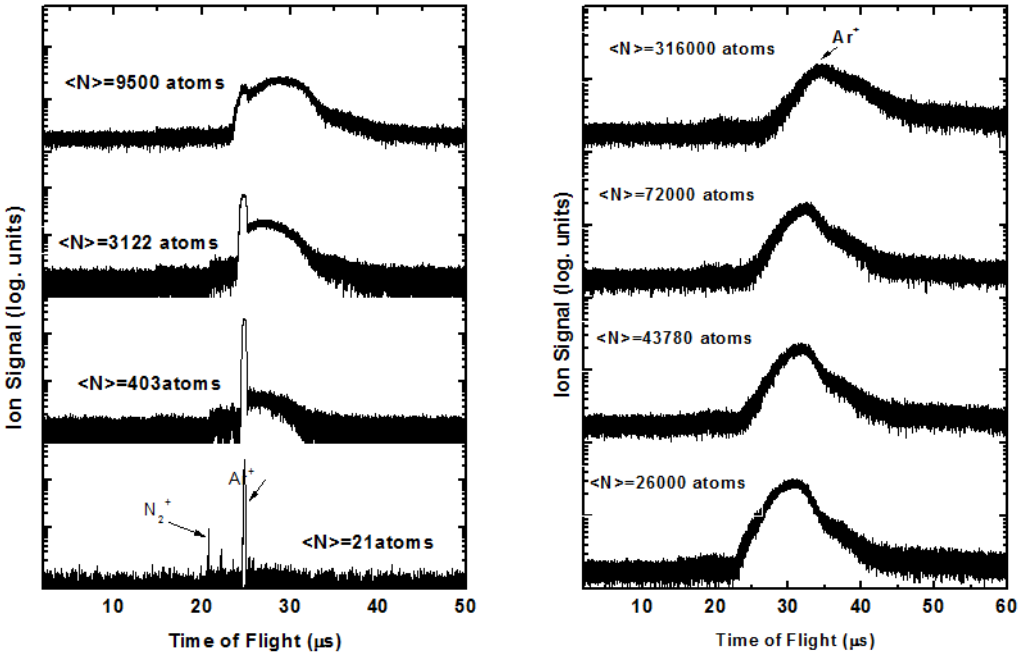

Figure 3.6: TOF of the XUV exploded Ar clusters as a function of the cluster size.

We were able to ionize up to Ar^{2+}, but no higher charge states were observed as shown in Fig. 3.7 which is a single shot TOF spectrum (8 bit digitizer); while in previously reported experiments, we observed charge states of Ar^{4+} [xxxv,xlii] In previous experiments we observed ion intensity ratios Ar3+/Ar+ ~200 so we would not expect to observe the higher charge states in Fig. 3.7 because of the poorer S/N. The data for Fig. 3.7 was averaged for 500 TOF oscilloscope traces without observing Ar^{3+}; while in the previous experiments we counted events for 5 hours using a time-delay, counting card (Comtec P7886S).

We have also repeated measurements of the ion energy distribution function for several cluster sizes as observed in Fig. 3.8. The sharp shoulder which increases in energy with increasing cluster size is indicative of a Coulomb explosion dominating the cluster dynamics. For cluster sizes approaching 100,000 atoms we observe a high-energy tail generated by the hydrodynamic expansion of a neutral plasma core in the cluster. This cluster size in argon is the beginning of a transition from Coulomb explosion in small clusters to hydrodynamic expansion in large ones. We will study this transition with more detail in proposed experiments.

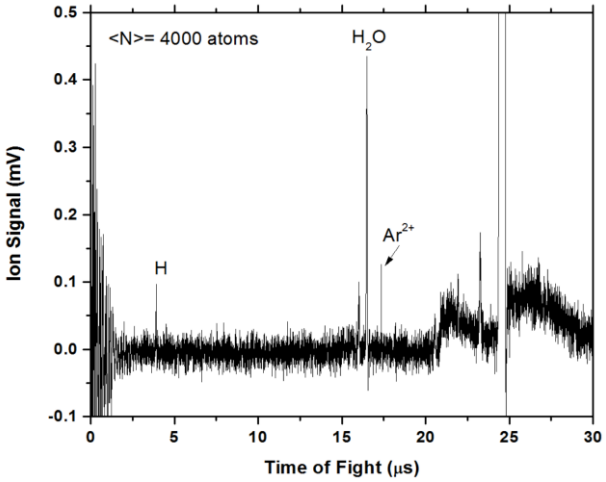

Figure 3.7: Using XUV we were able to ionize argon clusters up to Ar^{2+}.

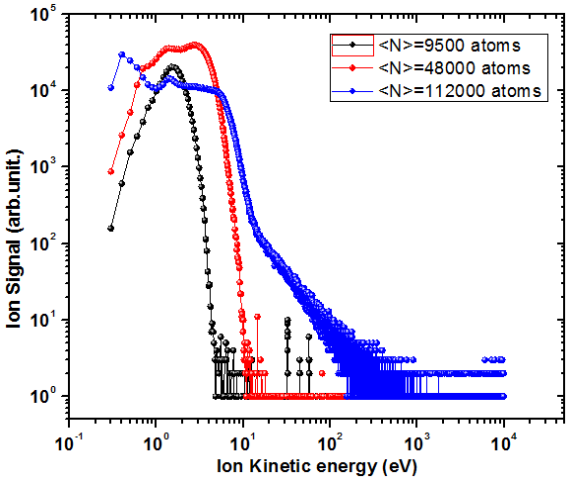

Figure 3.8: Argon ion kinetic energy as function of the average cluster size.

The second experiment was conducted on Xe clusters, and we reproduced the previously observed charge states above Xe^{3+}, which would be expected for ionization of atoms (IP Xe^{3+}-Xe^{4+} = 40.9 eV). As discussed in Sec. 2.3 we previously saw up to Xe^{8+} with a sharp drop in the intensities above Xe^{5+}. This is again observed in new experiments shown in Fig. 3.9. The estimates given in Sec. 2.3 for continuum lowering predict single photon ionization of Xe^{4+} but not for production of charge states above Z=5+. While these charge states were observed in FEL experiments for similar intensities (~ 10^{13} Wcm^{-2}), the fluences in the FEL experiments were ~10^2 larger than even our current ones (7 J cm^{-2} vs 80 mJ cm^{-2}) and a factor of 10^3 larger than our previous experiments.[xxxviii] We have now reproduced our previous observations we significantly different laser and XUV beam line conditions. We verified in both the previous and current experiments that IR light, perhaps leaking through pinholes in the Al filter, did not contribute to cluster heating. A glass slide was translated into the XUV beam following the Al filter. The slide completely blocks high harmonics but would transmit stay IR light and low harmonics normally blocked by the filter. The slide completely extinguished both the TOF signal and measurement on the XUV diode. We also reproduced our current XUV total energy measurements after the interaction zone (~5 nJ) with XUV diodes of different areas and capacitance.

While we have observed the same ion states as in FEL experiments, the intensities observed are very different. We observe a Xe^{+}/Xe^{2+} ratio of nearly 10, with factors of ~2 further decrease in population with increasing charge state. Because of the larger fluence in FEL experiments, depletion of neutral and lower charge state ions occurs such that at a cluster size of 30,000 atoms the population of Xe^{2+} is twice that of Xe^{+}, with only 20% decreases between charge states for more highly charged ions. This production of ions is supported by recent theory which includes continuum lowering, ionization from excited states of ions and atoms, and collisional ionization.[xxxix]

The confirmation of previous results is important because recent studies of XUV heating of clusters using harmonic light failed to observe charge states above Xe^{2+}.[xl] Because of the high contrast of THOR after the upgrade, there is no possibility of preheating of the clusters by prepulses in the laser. These would not produce harmonics. The XUV intensities and fluences between the two labs are very similar, but the Xe TOF spectrum reported was excited by the 13th and 15th harmonics produced in Xe gas with a S/N of ~50. Our experiments were conducted for predominantly 21st harmonic (25% 19th and 23rd observed) where we expected and observed production of Xe^{3+} for even atomic jets (eg. <N> = 1). Since the apparatus for the two experiments were similar, with similar fluences and powers in our current experiments we would expect similar results. We even used the same models of XUV diodes to measure the energy in the interaction region.

The TOF traces in this experiment are of a resolution sufficient to show five isotopes of Xe, an assurance of the quality of the new design of the TOF spectrometer (Fig. 3.5). The Xe ion kinetic energy measurements shown in Fig. 3.10 can be compared with those for Ar shown in Fig. 3.8.

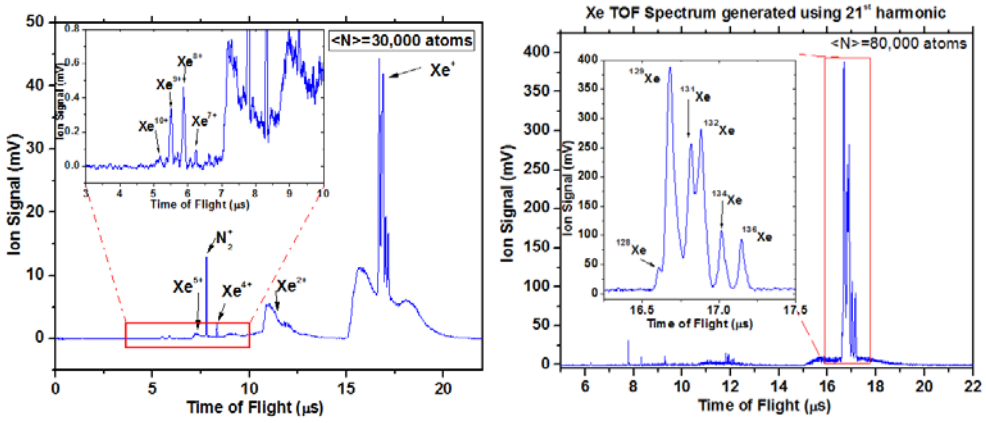

Figure 3.9: Xe TOF shows the highest charge we achieved, Xe^{10+} (left), and the TOF resolution as we resolved the xenon stable isotopes (right). The change in TOF results from different extractor voltages.

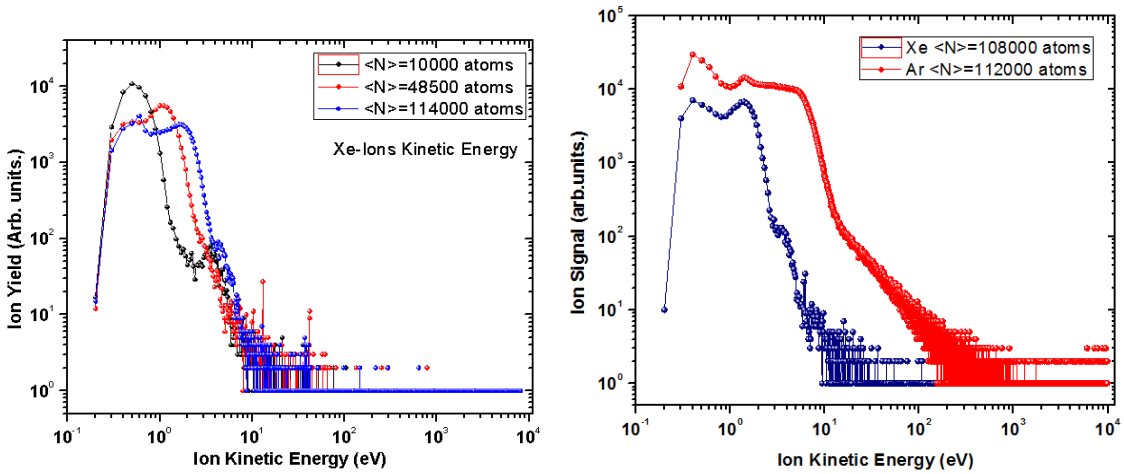

Figure 3.10: Xe ion kinetic energy versus the cluster size (left) and in comparison with the Ar ion kinetic energy for the same cluster size (right).

Our third experiment was to irradiate methane clusters with XUV in order to compare our results at photon energies = 33 eV with the previous results in SLAC experiments [xli] at photon energies of 800 and 2000 eV. The most dramatic difference between the two experiments is the intensity of the proton peak which is 3 times brighter than the hydrocarbon peaks when exciting with x-rays at LCLS. As observed in Fig. 3.11 for XUV light, the hydrogen fragmentation is much smaller. We observe CH^{5+} and larger cluster ions in both experiments, and the peak intensity increases with cluster size. For both experiments the cluster explosion is more energetic as observed by the increased peak widths as the cluster size increases, but we don't observe a strong forward-backward ion pedestal as observed for Xe in Fig. 3.9. Finally, we see that the height of the proton peak generated during the cluster explosion increases until a cluster size of ~30,000 molecules, and then it decreases. In the ion energy spectra we observe a transition between Coulomb and hydrodynamic explosion of the clusters at approximately the same cluster size.

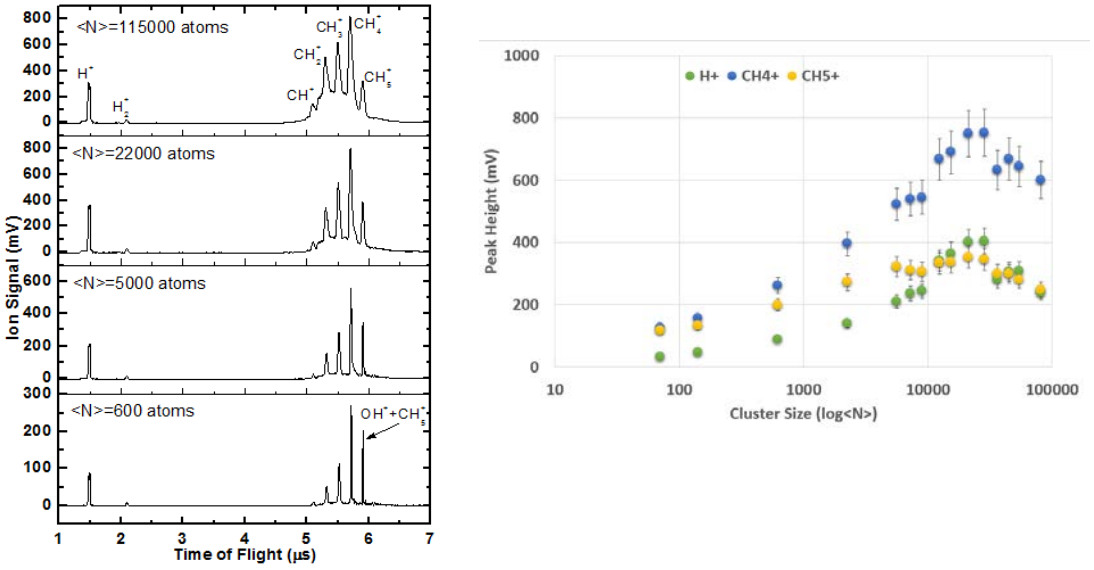

Figure 3.11: Ch_4 ion TOF versus the cluster size (left) and the trend in the proton peak we observe in comparison with the same trend of the CH_4^+ and CH_5^+(right).

Finally, we report data on nitrogen clusters. We are currently analyzing this data for physical insights into the expansion of these molecular nitrogen clusters, for comparison with our measurements of molecular methane clusters. Unlike for methane, we don't observe the formation larger ions such as N_3^+ which are observed in nitrogen discharges. We did not see any N^{2+} or higher charge states; we were only able to break the molecular bond in the N_2 molecule. This makes sense, knowing that the nitrogen is bonded covalently and needs at least 9.79 eV to break it. We did see a clear increase in the height of the backward- and forward-going ions, on either side of the main peak, that result from the cluster explosions, as characterized in the time-of-flight spectrometer Fig. 3.12.

We are hopeful that the explosion dynamics of nitrogen clusters might be clarified by analysis of many ion time-of-flight data traces as shown in Fig. 3.12, which are rich in features. For example, the base of the individual ion species, though originating from the same clusters, have different shapes. This indicates a potential difference in their generation during the cluster expansion process. Another feature is that the relative ratio of the N^+ and N_2^+ peak amplitudes varies with cluster size. We are comparing this data with similar data sets from methane.

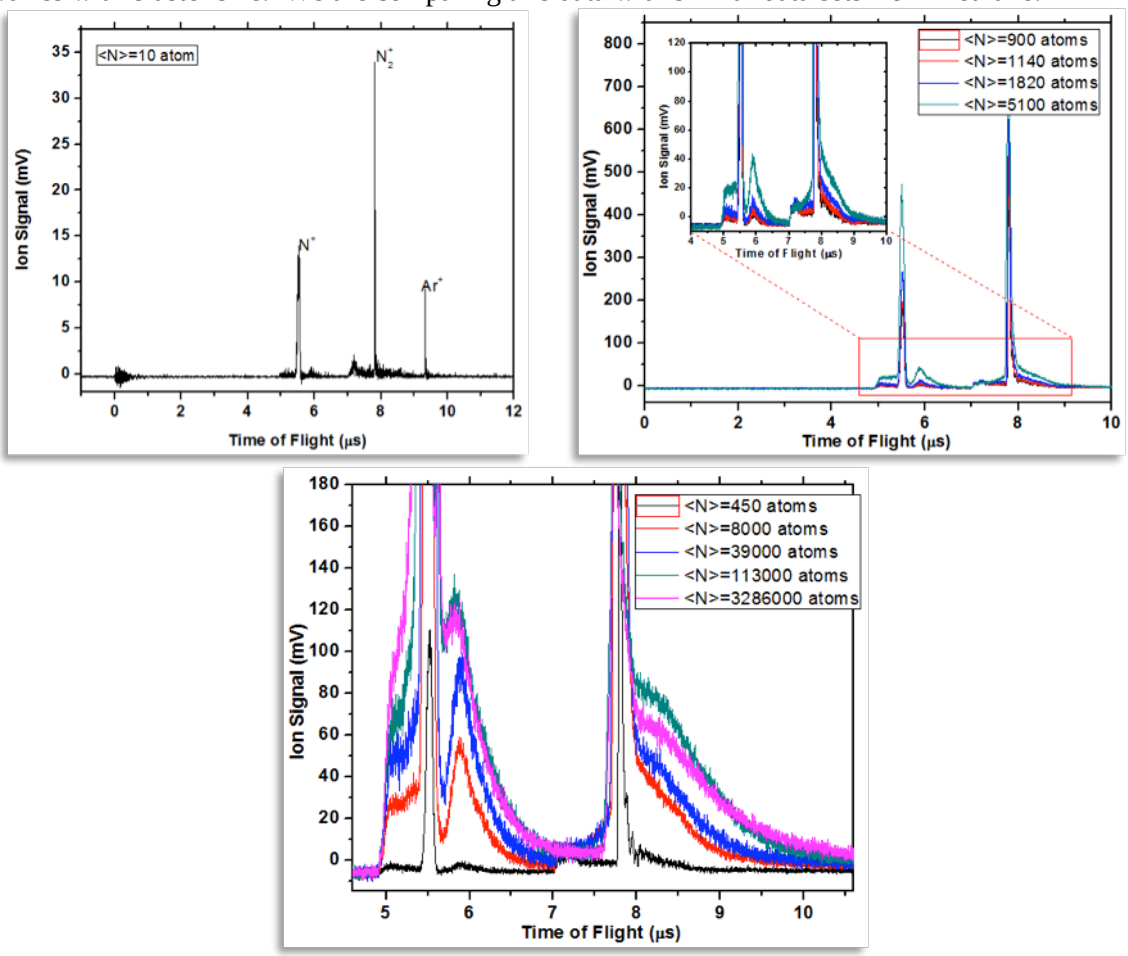

Figure 3.12: Nitrogen ion TOF shows the ionization of nitrogen molecule and nitrogen atom only (Top left), Cluster size effect on the explosion of both the forward and backward cluster peaks is shown (top right and bottom).

3.5 High-Intensity XUV Irradiation of Metal Oxide Nanoparticles, Generated by Laser Ablation of Microparticles

Previous experiments in this field, using van der Waals-bound gas nanoclusters as model targets, have identified anomalously high charge states of ions ejected from the cluster explosion – higher than would be achievable by single photon absorption in a gas [xxxv,xlii] It was speculated that these dense nanoclusters, when irradiated with a high intensity XUV light source, formed a dense nanoplasma which exhibited the phenomenon of continuum lowering, effectively lowering the potential barrier around each atom, and hence lowering the ionization energy of bound electrons.

If we model the continuum electron distribution in a solid-density plasma as uniformly distributed within a sphere of radius proportional to $n_i^{-1/3}$, where n_i is the ion density, we expect the amount of continuum potential lowering to be:

$$\Delta I_p = \frac{9}{10}\left(\frac{e^2}{\varepsilon_0}\right)\left(\frac{n_i}{48\pi^2}\right)^{1/3}(2Z-1) \qquad (1)$$

where e is the elementary charge, ε_0 is the vacuum permittivity, and Z is the average atomic number of the ions in the plasma. Therefore, if we use different metal oxides as target materials (e.g. SiO_2, TiO_2, ZrO_2, and SnO_2), and observe the highest resulting ionization state of the oxygen atoms, we expect continuum lowering to reduce the ionization energy depending upon the ionization potential of the metal atoms. For high Z metal atoms we should produce large ionization states as in Xe, with a resulting increase in the electron density and screening in the nanoplasma. Accordingly, we have designed an experiment using metal oxide nanoparticle targets, which will be irradiated by a high-intensity 38 nm pulse from the newly upgraded Texas High-intensity Optical Research (THOR) laser system. The results of this experiment will elucidate the role of continuum lowering in nanoclusters.

We will generate the target metal oxide nanoparticles using the laser ablation of microparticles (LAM) technique pioneered by Keto, Brock, and Becker [vii]. Accordingly, we have made significant progress in assembling and testing this apparatus in our lab. The full assembled apparatus is shown below, in Fig. 3.13.

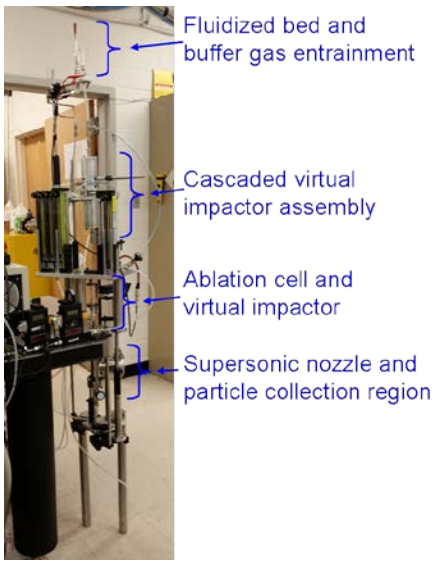

Figure 3.13. The fully assembled LAM apparatus, to be used to generate nanoparticle targets for our coherent XUV beamline.

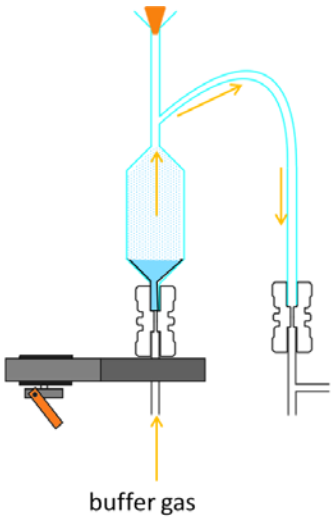

Figure 3.14 . Diagram of fluidized bed and buffer gas entrainment assembly.

The first part of the LAM apparatus is the fluidized bed and buffer gas entrainment assembly, shown in greater detail in Fig. 3.14. In this initial stage, we continuously agitate a reservoir of commercially available metal oxide microparticles (diameter about 2 μm) using a specially designed off-axis-weighted motor. At the base of the bed, there is a 250 μm orifice, through which we inject our He buffer gas. As the gas flows through the fluidized bed, a uniformly dense cloud of aerosolized microparticles forms in the reservoir above the bed. At this point, the microparticle cloud contains entrained single particles, as well as agglomerated groups of particles.

We then direct the buffer gas and particles through a cascaded pair of virtual impactors, which sort the particles by mass and discard particle agglomerates. Smaller particles follow the flow streamlines on the path of steepest decent through the pressure gradient, and remain in the major flow, while larger particles continue in a straight line into a probe with a much smaller flow. In the first stage, we discard oversized particles and agglomerates that end up in the probe's minor flow, while allowing the smaller, unagglomerated particles to pass through the major flow to the second stage. In the second stage, we discard all undersized particles that end up in the major flow, as well as any excess buffer gas, while keeping the standard-sized particles in the minor flow. We direct the resulting sorted particles to the ablation cell. Figure 3.15 shows a diagram of our cascaded virtual impactor assembly, while Figure 3.16 shows the results we achieved when we tested our virtual impactor assembly with Ag microparticles of diameter 1-2 μm.

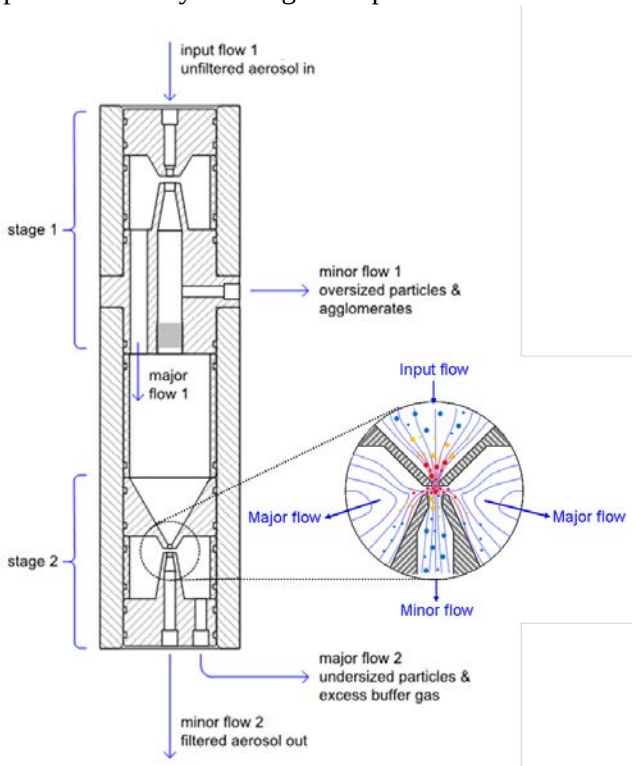

Figure 3.15. Diagram of cascaded virtual impactor assembly.

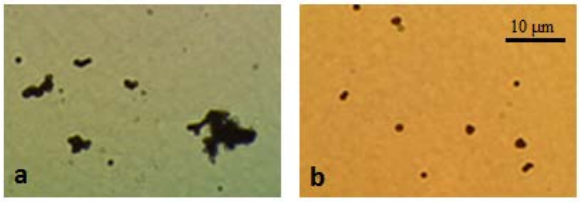

Figure 3.16. Ag microparticles of diameter 1-2 μm, as viewed under an optical microscope. We see that before sorting the particles (a), we have a considerable number of large agglomerates entrained in our buffer gas, whereas after passing through the cascaded virtual impactor assembly (b), the particles have a nearly uniform size distribution.

Once we have created a microparticle aerosol of uniform particle size, via our cascaded virtual impactor assembly, we direct the stream of particles into our ablation cell, shown in Figure 3.17. In the first half of the ablation region, we focus a 500 mJ, 532 nm, Q-switched pulsed laser into a line, using a cylindrical lens. The line focus ablates the microparticles in the aerosol, and the ablated material condenses into nanoparticles. We can control the resulting nanoparticle size by altering the density of the surrounding buffer gas.[**Error! Bookmark not defined.**]

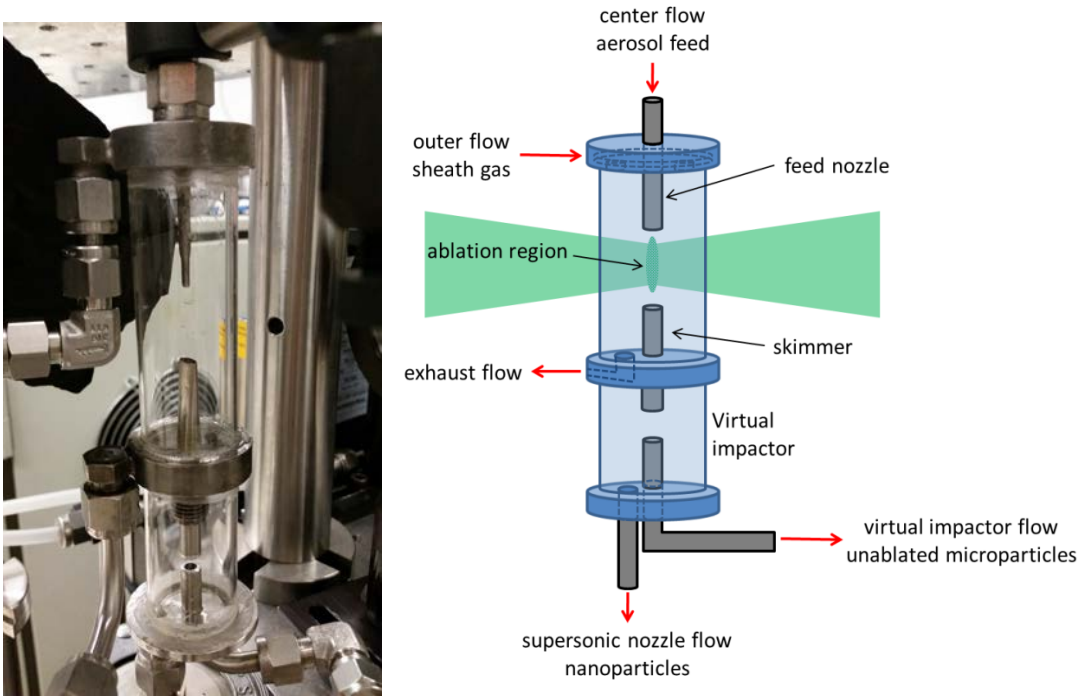

Figure 3.17 The ablation cell assembly on our LAM apparatus. The actual ablation cell (left) is shown next to a labeled diagram (right) describing its use.

The second part of the ablation cell is another virtual impactor, in which we separate the unablated microparticles from the nanoparticles. We direct major flow from this stage, containing our nanoparticles, through a 150 μm continuous flow supersonic nozzle, into a vacuum chamber, where we may collect and/or examine the resulting particle stream. For some experiments (below) we eliminated the lower virtual impactor and allowed both nanoparticles and microparticles in the aerosol flow to enter the target chamber.

3.6 Preliminary Results using LAM Source of Clusters

We have now successfully operated the LAM source on the target chamber. For these first preliminary experiments, we have used silver as the microparticle source, entrained in an atmospheric pressure N_2 aerosol. The mean size of Ag nanoparticles produced in atmosphere pressure N_2 aerosol has been measured previously to be 20 nm.[vii] The

flow velocity of the aerosol is 100 cm/s in the ablation cell and the ablation laser is focused to a 1 cm long line image. At the 10 Hz repetition frequency of the YAG laser, we ablate 10% of the aerosol stream. This alternating microparticle/nanoparticle aerosol is continuously expanded through the 150 μm supersonic nozzle into the target chamber. In order to hit the nanoparticle part of the jet, we must time the firing of THOR relative to the ablation laser. Results are shown in Fig. 3.18 which includes three, single-shot TOF spectra, one with no particles showing ionization of the N_2 gas, one showing the spectra when timed to hit a microparticle, and one when timed to hit nanoparticles. We observe several features in each spectra. We expect no N_2 clustering in this jet with the 150 μm flat plate nozzle, so each N_2 ion peak is a doublet due to the forward/backward direction of the dissociated N_2 molecules, relative to the TOF extraction field direction. When timed to hit a microparticle, we obtain the silver ion signal only every ~100 laser shots. Each spectrum is then from a single, isolated microparticle. This low rate results from the low microparticle density in the jet (~10^4 cm^{-3} in the ablation cell), and the small focal volume of the THOR laser. We observe two dominant peaks in the TOF spectrum, Ag^+, and H^+. The latter comes from the de-agglomerating coating placed on the particles by the manufacturer. The both ion peaks are very broad due to the large explosion energy of the microparticle. There is no indication of atomic silver in the background as we would expect. Under higher gain we can observe the N_2 peaks observed in the aerosol spectrum.

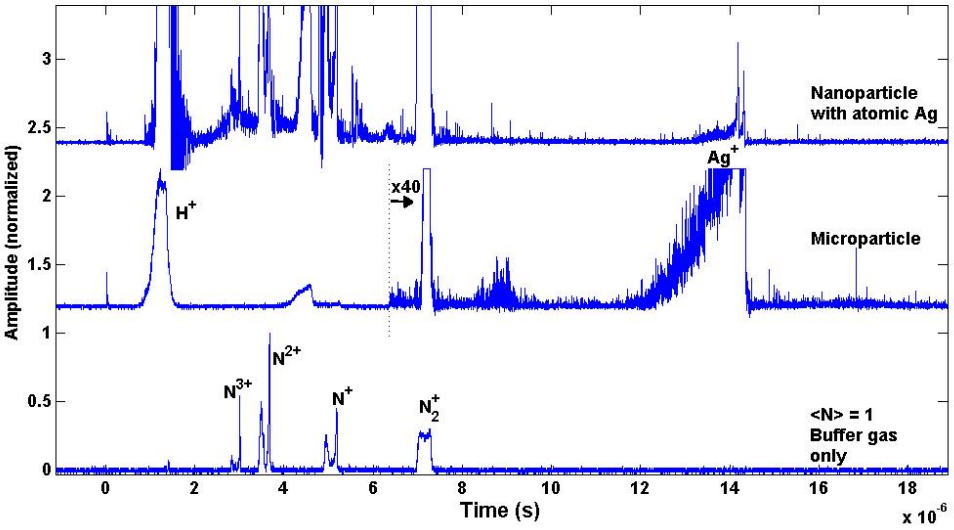

Fig. 3.18. TOF spectra following interaction of 50 mJ pulses of 800 nm light from THOR with Ag nanoparticles produced by LAM. Three single-shot spectra are shown, that of the aerosol gas without particles, spectra from a single, exploding microparticle and from an exploding nanoparticle. We see a broad H^+ peak and at 4.8 μs a broad carbon peak from both particles.

When THOR is timed to hit nanoparticles, the TOF is distinctly different from that of microparticles. The Ag^+ peak has a broad pedestal due to the exploding nanoparticle, but we also observe sharp peaks from the two isotopes of Ag atoms. These atoms are part of the aerosol background because of the evaporation of Ag atoms during the ablation process. When the laser focus is adjusted onto the jet, we hit Ag nanoparticles every few laser shots. We previously estimated that ~10^5 of the 20 nm dia. nanoparticles are produced for each microparticle.[vii] In addition, we expect the nanoparticles to be

focused to a diameter of ~40 μm by the supersonic nozzle.[xliii] Both effects increase the "hit" rate for nanoparticles relative to the microparticles but not my the ratio of the increase in average particle density. We know that in the ablation process the nanoparticle cloud originating from an ablated microparticle expands until the work done on the aerosol gas equals the ablation laser energy absorbed by the microparticle.[**Error! Bookmark not defined.**] This results in a diameter ~100 μm of the nanoparticle cloud. Diffusion then disperses the nanoparticles further, but the density of the nanoparticles is not uniform in the aerosol volume.[xliv] Because the nanoparticles are grouped in the flow we are not hitting single, individual nanoparticles with the THOR laser beam, but because the size of the nanoparticles is monodisperse we may be able to determine the number of nanoparticles by the number of ions collected. This will require additional data analysis to determine. The next phase of our experiments with Ag nanoparticles will use the XUV laser beam.

3.6 Papers supported during this past grant period

1. K. Hoffmann, B. Murphy, B. Erk, A. Helal, N. Kandadai, J. Keto, and T. Ditmire, "High intensity femtosecond XUV pulse interactions with atomic clusters," High Energy Density Phys. **6**, 185 (2010).
2. K. Hoffmann, B. F. Murphy, N. Kandadai, B. Erk, A. Helal J. Keto, and T. Ditmire, "Rare-gas-cluster explosions under irradiation by intense short XUV pulses" *Phys. Rev. A*, **83**, 043203 (2011).
3. R. D. Morgan, J. W. Keto and T. Ditmire, "Colloidal nanoparticles : a promising gain medium for high average power lasers, " J. Opt. Soc. B, **28**, 2726-2734(2011).
4. B. Erk, K. Hoffmann, N. Kandadai, A. Helal, J. Keto, and T. Ditmire "Observation of shells in Coulomb explosions of rare-gas clusters" *Phys. Rev. A* **83**, 043201 (2011).
5. W. Bang, H. J. Quevedo, G. Dyer, J. Rougk, I. Kim, M. McCormick, A. C. Bernstein, A. and T. Ditmire, "Calibration of the neutron detectors for the cluster fusion experiment on the Texas Petawatt Laser" *Rev. Sci. Instruments* **83**, 063504 (2012).
6. H. Thomas, N. Kandadai, K. Hoffmann, A. Helal, J. Keto, B. Iwan, N. Timneanu, J. Andreasson, M. Seibert, D. van der Spoel, J. Hajdu, S. Schorb, T. Gorkhover, D. Rupp, M. Adolph, T. Möller, G. Doumy, L.F. DiMauro, C. Bostedt, J. Bozek, M. Hoener, B. Murphy, N. Berrah and T. Ditmire "Explosions of Xe-clusters in ultra-intense femtosecond x-ray pulses from the LCLS X-ray Free Electron Laser" *Phys. Rev. Lett.* **108**, 133401 (2012).
7. Nirmala K. Kandadai, "Interaction of clusters with fs x-ray free electron lasers," Ph.D. Dissertation, The University of Texas at Austin, August, 2012.
8. W. Bang, M. Barbui, A. Bonasera, G. Dyer, H. J. Quevedo, K. Hagel, K. Schmidt, F. Consoli, R. De Angelis, P. Andreoli, E. Gaul, A. C. Bernstein, M. Donovan, M. Barbarino, S. Kimura, M. Mazzocco, J. Sura, J. B. Natowitz, and T. Ditmire, "Temperature Measurements of Fusion Plasmas Produced by Petawatt-Laser-Irradiated D^2-He^3 or CD_4-He^3 Clustering Gases" *Phys. Rev. Lett.* **111**, 055002 (2013).
9. W. Bang, G. Dyer, H. J. Quevedo, A. C. Bernstein, E. Gaul, M. Donovan, and T. Ditmire, "Optimization of the neutron yield in fusion plasmas produced by Coulomb explosions of deuterium clusters irradiated by a petawatt laser" *Phys. Rev. E* **87**, 023186 (2013).
10. N. Timneanu, B. Iwan, J. Andreasson, M. Bergh, M. Seibert, C. Bostedt, S. Schorb, H. Thomas, D. Rupp, T. Gorkhover, M. Adolph, T. Möller, A. Helal, K. Hoffmann, N. Kandadai, J. Keto, T. Ditmire, "Fragmentation of clusters and recombination sinduced by intense ultrashort X-ray laser pulses," Proc. SPIE Vol. 8777, p. 87770J1-J7, (2013).
11. N. Kandadai, K. Hoffmann, A. Helal, H. Thomas, J. Keto, T. Ditmire, B. Iwan, N. Timneanu,

J. Andreasson, M. Seibert, D. van der Spoel, J. Hajdu, S. Schorb, T. Gorkhover, D. Rupp3, M. Adolph, T. Möller, G. Doumy, L.F. DiMauro, C. Bostedt, J. Bozek, M. Hoener, B. Murphy, N. Berrah, "Explosion of Methane Clusters in Intense FEL Pulses", to be published *Phys. Rev. Lett.*

12. N. Kandadai, K. Hoffmann, A. Helal, H. Thomas, J. Keto, J. Andreasson, ,B. Iwan[3], M. Seibert[3], N. Timneanu[3], J. Hajdu[3], M. Adolph, T. Gorkhover, D. Rupp, S. Schorb, T. Möller, G. Doumy, L.F. DiMauro, M. Hoener, B. Murphy, N. Berrah, J. Bozek, C. Bostedt and T. Ditmire, "Explosion of Xe doped CH_4 clusters in ultra-intense femtosecond x-ray pulses", to be submitted to *Phys. Rev. Lett.*

13. N. Kandadai, K. Hoffmann, A. Helal, H. Thomas, J. Keto, T. Ditmire, B. Iwan, N. Timneanu, J. Andreasson, M. Seibert, D. van der Spoel, J. Hajdu, S. Schorb, T. Gorkhover, D. Rupp[3], M. Adolph, T. Möller, G. Doumy, L.F. DiMauro, C. Bostedt, J. Bozek, M. Hoener, B. Murphy, N. Berrah, "CH_4 and CD_4 cluster interaction with X-ray photons," to be submitted *Phys. Rev.*

Appendix 1: Bibliography and References Cited

*i. A. W. Castleman and R. G. Keesee, "Gas-Phase Clusters: Spanning the States of Matter", Science **241**, 36 (1988).*

*ii. O. F. Hagena and W. Obert, "Cluster Formation in Expandion Supersonic Jets: Effect of Pressure, Temperature, Nozzle Size, and Test Gas", J. Chem. Phys. **56**, 1793 (1972).*

*iii. T. G. Dietz, M. A. Duncan, D. E. Powers, and R. E. Smalley, J. Chem. Phys. **74**, 6511 (1981).*

*iv. K. LaiHing, R. G. Wheeler, W. L. Wilson, and M. A. Duncan, J. Chem. Phys. **87**, 3401 (1987).*

*v. Ching-Bo Juang, Hong Cai, Michael F. Becker, John W. Keto, and James R. Brock, "Synthesis of ultrafine glass particles by laser-induced fragmentation", Appl. Phys. Lett. **65.1**, 40(1994).*

*vi. H. Cai, N. Chaudhary, J. Lee, M. F. Becker, J. R. Brock, and J. W. Keto, "Generation of Metal Nanoparticles by Laser Ablation of Microspheres, J. of Aerosol Science **29**, 627-636 (1998).*

*vii. W.T. Nichols, D.E. Henneke, G. Malyavanatham, M.F. Becker†, J.R. Brock, J.W. Keto, and H. D. Glicksman, "Large scale production of nanocrystals by laser ablation of aerosols of microparticles," Appl. Phys. Lett. **78**, 1128-1130(2001).*

*viii. V, Ayvazyan, et al. "Generation of GW radiation pulses from a VUV free-electron laser operating in the femtosecond regime" Phys. Rev. Lett. **88**, 104802 (2002).*

ix P. Emma et al., in Proceedings of the 2009 Particle Accelerator Conference, Vancouver, BC, Canada.

*x. B. F. Murphy, K. Hoffmann, A. Belilopetski, J. Keto, and T. Ditmire, "Explosion of Xenon Clusters Driven by Intense Femtosecond Pulses of Extreme Ultraviolet Light" Phys. Rev. Lett. **101**, 203401 (2008).*

xi. K. Hoffmann, B. Murphy, N. Kandadai, B. Erk, A. Helal, J. Keto, and T. Ditmire , Rare gas Cluster Explosions with intense short pulse XUV Light, Phys. Rev. A, in preparation

xii. J. Hadju et al. "Structural Studies of Single particles and Biomolecules" in LCLS: The First Experiments, Sept. 2000.

*xiii. D. R. Symes, M. Hohenberger, A. Henig, and T. Ditmire, "Anisotropic Explosions of Hydrogen Clusters under Intense Femtosecond Laser Irradiation" Phys. Rev. Lett. **98**, 123401 (2007).*

*xiv. T. Ditmire, T. Donnelly, A. M. Rubenchik, R. W. Falcone, and M. D. Perry, "The Interaction of Intense Laser Pulses with Atomic Clusters," Phys. Rev. A **53**, 3379 (1996).*

*xv. T. Ditmire, et al., "High energy ion explosion of atomic clusters: Transition from molecular to plasma behavior", Phys. Rev. Lett. **78**, 2732-2735 (1997).*

*xvi. J. Purnell, E. M. Snyder, S. Wei, and A. W. Castleman, Jr., "Ultrafast Laser-Induced Coulomb Explosion of Clusters with High Charge States", Chem. Phys. Lett. **229**, 333 (1994).*

*xvii. H. Wabnitz et al. Nature **420**, 482 (2002).*

xviii. T. Laarmann et al., Phys. Rev. Lett. 95, 063402 (2005).

xix. C. Bostedt et al., Phys. Rev. Lett. 100, 133401 (2008).

*xx. R. Santra and C. H. Greene, Phys. Rev. Lett. **91**, 233401 (2003).*

*xxi. C. Siedschlag and J-M Rost, Phys. Rev. Lett. **93**, 043402 (2004).*

*xxii. I. Georgescu, U. Saalmann, and J. M. Rost, Phys. Rev. A **76**,043203 (2007).*

xxiii. C. Jungreuthmayer, L. Ramunno, J. Zanghellini, and T. Brabec, J. Phys. B: At. Mol. Opt. Phys. 38, 3029 (2005).

xxiv. Hans R. Griem, Plasma Spectroscopy (McGraw Hill, New York, 1964).

xxv. R.P. Drake, High Energy Density Physics: Fundamentals, Inertial Fusion and Experimental Astrophysics, (Springer-Verlag, Berlin, 2006).

*xxvi. K. W. Madison, R. Fitzpatrick, P. K. Patel, D. Price, T. Ditmire, "The role of laser pulse duration in Coulomb explosions of deuterium cluster targets" Phys. Rev. A **70**, 053201 (2004).*

*xxvii. B. N. Breizman, A. V. Arefiev, "Electron response in laser-irradiated microclusters", Plas. Phys. Rep. **29**, 593 (2003).*

*xxviii. R. F. Schmalz, Phys. Fluids **28**, 2923 (1985).*

*xxix. K. W. Madison, P. K. Patel, D. Price, A. Edens, M. Allen, T. E. Cowan, J. Zweiback, and T. Ditmire, "Fusion neutron and ion emission from laser induced explosions of deuterium and deuterated methane clusters" Phys. Plas. **11**, 270 (2004).*

*xxx. I. Last and J. Jortner, J. Chem. Phys. **121**, 8329 (2004).*

xxxi. M. Hohenberger, D. R. Symes, K. W. Madison, A. Sumeruk, G. Dyer, A. Edens, W. Grigsby, G. Hays, M. Teichmann, and T. Ditmire, Phys. Rev. Lett. 95, 195003(2005).

*xxxii. H. Thomas, N. Kandadai, K. Hoffmann, A. Helal, J. Keto, T. Ditmire, B. Iwan, N. Timneanu, J. Andreasson, M. Seibert, D. van der Spoel, J. Hajdu, S. Schorb, T. Gorkhover, D. Rupp[3], M. Adolph, T. Möller, G. Doumy, L.F. DiMauro, C. Bostedt, J. Bozek, M. Hoener, B. Murphy, N. Berrah, "Explosion of Xe-clusters in ultra-intense femtosecond x-ray pulses from the free-electron-laser LCLS", Phys. Rev. Lett. **108**, 133401(2012).*

xxxiii. H. Thomas, N. Kandadai, K. Hoffmann, A. Helal, J. Keto, B. Iwan, N. Timneanu, J. Andreasson, M. Seibert, D. van der Spoel, J. Hajdu, S. Schorb, T. Gorkhover, D. Rupp[3], M. Adolph, T. Möller, G. Doumy, L.F. DiMauro, C. Bostedt, J. Bozek, M. Hoener, B. Murphy, N. Berrah, P. Di Cintio[7], C. Gnodthke[7], U. Saalmann[7], J. Rost" and T. Ditmire, "Explosion of Methane clusters in intense x-ray FEL pulses pulses", submitted Phys. Rev. Lett.

xxxiv. I. Last, J. Jortner, Nuclear Fusion Driven by Coulomb Explosion of Methane Clusters", J. Phys. Chem. A, 106 (45), 10877-10885, (2002). M. Hohenberger, et al., Phys. Rev. Lett. 95, 195003(2005).

xxxv. K. Hoffmann, B. F. Murphy, N. Kandadai, B. Erk, A. Helal J. Keto, and T. Ditmire, "Rare-gas-cluster explosions under irradiation by intense short XUV pulses" Phys. Rev. A, 83, 043203 (2011).

*xxxvi. B.Erk, K. Hoffmann, B. F. Murphy, N. Kandadai, A. Helal, J. Keto, and T. Ditmire, "Observation of shells in Coulomb explosion of rare-gas clusters", Physical Review A **83,** 043201 (2011).*

*xxxvii. T. Ditmire et al., "High Energy Ion Explosion of Atomic Clusters: Transition from Molecular to Plasma Behavior", PRL, **78**, 14 (1997).*

*xxxviii. H. Wabnitz, et al., "Multiple ionization of atomic clusters by intense soft x-rays from a free electron laser, Nature **420**, 482(2002).*

xxxix. E. Ackad, N. Bigaouette, K. Briggs, and L. Ramunno, "Clusters in Intense XUV pulses: Effects of cluster size on expansion of dynamics and ionization," Phys. Rev. A83, 063201(2011).

*xl. B. Shutte, M. Arbeiter, Th Fennel, M.J.J. Vrakking, and A. Rouzee, "Rare-gas Clusters in Intense Extreme-Ultraviolet Pulses from a High-Order Harmonic Source," Phys. Rev. Lett. **112**, 073003(2014).*

xli. N. Kandadai et al., "Explosion of Methane Clusters Driven by Intense X-Ray FEL Pulses" OSA/CLEO 2011.

*xlii. B.F. Murphy, K. Hoffmann, A. Belolipetski, J. Keto, and T. Ditmire, "Explosion of Xenon clusters driven by intense femtosecond pulses of Extreme ultraviolet light," PRL **101,** 203401(2008).*

*xliii. Andre D. Albert, Michael F. Becker, John W. Keto, Desiderio Kovar, "Low Temperature, Pressure-Assisted Sintering of Nanoparticulate Silver Films," Acta Materialia **56**, 1820-1829(2008).*

*xliv. Gokul Malyavantham, Daniel T. O'Brien, Michael F. Becker, John W. Keto, and Desiderio Kovar, "Au-Cu nanoparticles produced by laser ablation of mixtures of Au and Cu microparticles," J. Nanoparticle Res. **6**, 661-664(2005)*